Energy Conversion and Management 293 (2023) 117454

Contents lists available at ScienceDirect

Energy Conversion and Management

journal homepage: www.elsevier.com/locate/enconman

Advances in solar thermal power plants based on pressurised central receivers and supercritical power cycles

M.J. Montes [a,*], R. Guedez [b], J.I. Linares [c], M.A. Reyes-Belmonte [d]

[a] E.T.S. Ingenieros Industriales - UNED, C/Juan del Rosal 12, 28040 Madrid, Spain
[b] Department of Energy Technology, KTH Royal Institute of Technology, Brinellvägen 68, 100 44 Stockholm, Sweden
[c] ICAI School of Engineering, Comillas Pontifical University, Alberto Aguilera, 25, 28015 Madrid, Spain
[d] Department of Chemical and Energy Technology, School of Experimental Sciences and Technology (ESCET), Rey Juan Carlos University, 28933 Móstoles, Madrid, Spain

ARTICLE INFO

Keywords:
Solar thermal power plant
Microchannel receiver
Radial configuration
Supercritical power cycle
Supercritical fluid
Pressurised gas

ABSTRACT

This work addresses the comparative thermo-economic study of different configurations of solar thermal power plants, based on supercritical power cycles and pressurised central receiver systems. For all the cases examined, two innovations are introduced in the solar subsystem, compared to other similar studies. Firstly, the heat transfer fluid in the receiver is either a pressurised gas or a supercritical fluid. Secondly, the receiver is composed of compact structures performing as absorber panels, arranged in a radial configuration. The investigation considers different supercritical CO_2 recompression cycles of 50 MW_e, including a novel proposal of a directly coupled cycle with heat input downstream of the turbine. Furthermore, the study evaluates different heat transfer fluids in the receiver, specifically CO_2, N_2, and He, concluding that the former is preferred due to its better thermal performance.

The main results show that an increase in the receiver inlet pressure yields to a reduction in its size, favouring the thermal efficiency but penalising the optical efficiency of the solar field. Therefore, optimal working pressures may exist for each configuration, depending on the operating temperature. When comparing the optimal configurations, it is observed that the plant based on the intercooling cycle demonstrates the highest overall efficiency, reaching 32.05%. At last, an economic analysis is conducted to assess the viability of the identified optimal configurations. In this regard, the plant based on the partial-cooling cycle exhibits the lowest levelised cost of electricity at 0.15 $/kWh. This is primarily due to its lower investment cost. The innovative directly coupled cycle follows closely with a cost of 0.17 $/kWh, driven by its high electricity production resulting from its low self-consumption.

1. Introduction

The current context has highlighted the need to achieve a sustainable, secure and competitive energy supply, independent of fossil fuels and based on several energy sources. Within this energy mix, Concentrating Solar Power (CSP) can play a relevant role. According to IRENA [1], between 2010 and 2021, the Levelised Cost of Electricity (LCOE) of Solar Thermal Power Plants (STPPs) decreased by 68%, from 0.358 $/kWh$_e$ to 0.114 $/kWh$_e$. This was mainly due to lower total installed costs (down 64%), higher capacity factors (up 17%), a reduction in operating and maintenance costs (down 10%) and a reduction in the Weighted Average Capital Cost (WACC) (down 9%). It is important to note that the decrease in LCOE over the last decade has been mainly driven by a reduction in the investment and Operation and Maintenance (O&M) costs. While LCOE can be reduced by reducing costs, there is a second approach to make CSP competitive: increasing the total STPP efficiency. This is the path set out by the Gen3 CSP Roadmap [2], and in this line, the use of supercritical carbon dioxide (sCO_2) cycles is a key element.

1.1. Integration schemes based on solar central receiver systems coupled to sCO_2 cycles

The Gen3 CSP Roadmap proposes three different STPP configurations, all of them based on the coupling between a sCO_2 cycle and a Central Receiver System (CRS) [2]. The differing element between the proposed schemes is the Heat Transfer Fluid (HTF) in the central

* Corresponding author.
E-mail address: mjmontes@ind.uned.es (M.J. Montes).

https://doi.org/10.1016/j.enconman.2023.117454
Received 22 May 2023; Received in revised form 13 July 2023; Accepted 23 July 2023
Available online 28 July 2023

Nomenclature

Acronyms

AEP	Annual Electricity Production
AC	Auxiliary Compressor
C	Compressor
CF	Capacity Factor
CHE	Compact Heat Exchanger
CRF	Capital Recovery Factor
CRS	Central Receiver System
CSP	Concentrating Solar Power
DNI	Direct Normal Irradiation
HTF	Heat Transfer Fluid
HTR	High Temperature Recuperator
HX	Heat Exchanger
LCOE	Levelised Cost of Electricity
LTR	Low Temperature Recuperator
MC	Main Compressor
NREL	National Renewable Energy Laboratory
O&M	Operation and Maintenance
OMC	Operation and Maintenance Costs
PBT	Packed Bed Thermocline
PEC	Purchase Equipment Cost
PCHE	Printed Circuit Heat Exchanger
PFHE	Plate Fin Heat Exchanger
PHE	Plate Heat Exchanger
sCO_2	Supercritical Carbon Dioxide
STPP	Solar Thermal Power Plant
T	Turbine
TCC	Total Capital Cost
TES	Thermal Energy Storage
TM	Turbomachinery
TRM	Thermal Resistance Model
WACC	Weighted Average Capital Cost

Latin letters

CO_2	Carbon Dioxide
h	Enthalpy (J kg^{-1})
He	Helium
m	Mass flow rate (kg s^{-1})
N_2	Nitrogen
ΔP	Pressure drop (Pa)
P	Pressure (Pa)
$\dot{Q}$	Thermal power (W)
R	Thermal resistance (K W^{-1}) / Ideal gas constant (J kg^{-1} K^{-1})
T	Temperature (K)
v	Velocity (m s^{-1})
$\dot{W}$	Electrical power (W)

Greek Letters

η	Efficiency
Δ	Differential
δ	Angle (rad)

Subscripts

amb	Ambient
e	Electrical
LMTD	Logarithmic Mean Temperature Difference
opt	Optical
out	Outlet
s	Sun
th	Thermal
0	Reference

receiver, specifically molten salt, solid particles or gas [3]. For any of these options the solar receiver is indirectly coupled to the power cycle through a heat exchanger [4,5] between the HTF from the receiver and the sCO_2 from the cycle. In addition to indirectly coupled schemes, there are studies that propose direct coupling between the solar receiver and the supercritical cycle [6,7], thus using sCO_2 in the solar receiver. A brief description of the state-of-the-art for each of these four schemes is given in the next paragraph.

The scheme of molten salt central receiver coupled to a sCO_2 cycle, is the most studied, as it is the logical evolution of current commercial tower plants. In these plants, the molten salt also performs as storage fluid in the Thermal Energy Storage (TES) system, both in a direct two-tank or a thermocline configuration [8,9]. In order to improve the performance of the supercritical cycle, it is necessary to work at higher temperature than that of commercial STPPs, about 700 °C at the outlet of the solar receiver; hence, the use of advanced ternary salts is necessary [10].

The STPP based on a particle central receiver coupled to a sCO_2 cycle, is analysed in several works [11,12]. Regarding the solar receiver, there are two different concepts [13]: directly irradiated and indirectly irradiated. Direct particle receivers include free-falling, obstructed-flow, centrifugal and fluidised designs. Indirect particle receivers include gravity-driven flow in enclosures and fluidised flow in tubes. One of the key features of this scheme is the possibility of directly storing the particles in tanks, providing the plant with dispatchability [14]. And the main challenge for the technical feasibility of these plants is the development of a heat exchanger to transfer the thermal energy to the sCO_2 in the cycle [15,16].

The global scheme consisted of a pressurised gas receiver coupled to a sCO_2 cycle, has been extensively analysed in [17]. Regarding the storage system in this scheme, there are different proposals, being worth to highlight the works about the design and simulation model of a sensible Packed Bed Thermocline (PBT) for pressurised air [18,19].

At last, there are several studies on direct integration between the solar tower system and the power block, employing supercritical CO_2 as working fluid in both systems. To achieve direct coupling, it is necessary to develop solar receivers and storage systems capable of withstanding high temperatures and pressures. There are already several designs and prototypes of solar receivers for supercritical fluids, as will be discussed in section 1.2. Regarding storage in the case of using a supercritical fluid in the solar field, an indirect molten salt TES is the most conventional storage option. However, there are also proposals [6,7] for a thermocline system based on a set of smaller individual vessels, to reduce the wall thickness.

The work presented in this paper focuses on the schemes based on a pressurised gas or supercritical fluid in the central receiver system and a sCO_2 cycle, considering both directly and indirectly coupled schemes, the last one shown in Fig. 1. This work has focused on the integration between the solar receiver and the power cycle in a stand-alone STPP, without including the TES. As the comparative analysis has been carried out at design conditions, the TES only introduces the solar field oversizing, but no differences between the STPP configurations considered.

In the next two sections of the introduction, an analysis of the state-of-the-art is conducted for the two main systems in the integration schemes being studied: the solar receiver and the power cycle.

1.2. The solar central receiver for pressurised gases and supercritical fluids

Pressurised gas solar receivers have been studied for decades [17].

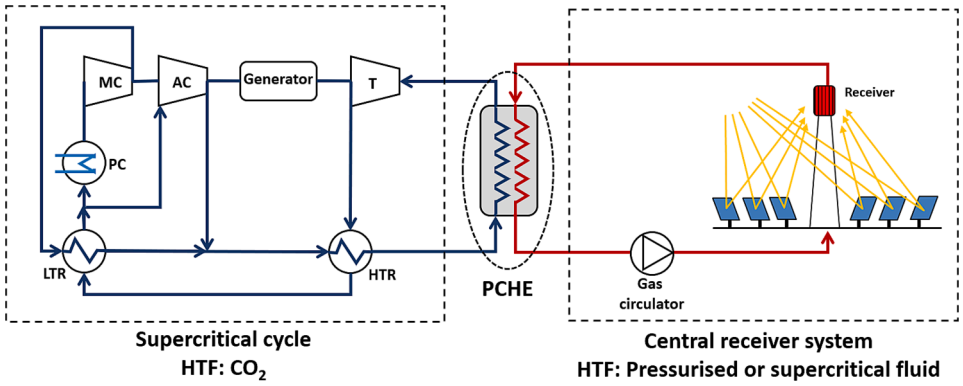

Fig. 1. Scheme of STPP based on a pressurised gas or supercritical fluid in the central receiver system, indirectly coupled to a sCO_2 cycle. T, Turbine; MC, Main Compressor; AC, Auxiliary Compressor; LTR, Low Temperature Recuperator; HTR, High Temperature Recuperator; PC, Pre-Cooler; PCHE, Printed Circuit Heat Exchanger.

The most traditional concept is the tubular gas receiver, which has been improved to work with gaseous or supercritical fluids. These improvements include the use of multi-layered tubes consisting of Inconel and copper to enhance radial and circumferential heat transfer [20,21] or bladed configurations that perform as a light trapping to reduce heat losses, when working at high temperatures [22]. In addition to tubular designs, the microchannel receiver is a more recent concept that is being extensively studied for both pressurised gases and supercritical fluids. It offers the advantage of increasing the heat transfer area between the HTF and the irradiated receiver walls.

This type of receiver is based on compact structures such as those used in Compact Heat Exchangers (CHEs) [23], basically Plate Heat Exchanger (PHE), Plate-Fin Heat Exchanger (PFHE), Printed Circuit Heat Exchanger (PCHE), the plates being diffusion bonded [24,25]. Within the technical literature, three designs based on this concept are highlighted. The first design was developed by the Oregon State University and consisted of an array of modular microchannel cells [26]. The second design was a 3 MW_{th} plain rectangular fin-type microchannel receiver, arranged in a cavity configuration [27]. At last, the National Renewable Energy Laboratory (NREL) proposed a wavy fin microchannel receiver [28]. This design served as the basis for manufacturing a prototype in a cavity configuration. Additionally, a model for an external receiver was simulated based on this concept.

The design adopted for this work is a microchannel receiver, in which the absorber panels consist of compact structures of increasing compactness, arranged in a radial configuration [29]. This design has been validated and analysed in [30,31], and it is depicted in Fig. 2, with the configuration and dimensions optimised for the thermal power and fluid working conditions (temperature and pressure) corresponding to the comparative study carried out in this work. The radial configuration presents three features that are very suitable for working with gaseous or supercritical fluids at high temperature: the prismatic cavities between two consecutive panels perform as macroscopic light trapping geometries, reducing the view factor and therefore the heat losses to the outside; the irradiated external surface area is larger compared to an external receiver of the same diameter and height; finally, the panels are irradiated on both sides. Regarding the increased compactness, the main advantage is improving heat transfer only in the areas with more challenging boundary conditions (higher irradiation and/or hotter heat transfer fluid with worse thermal properties), without excessively penalising the pressure drop due to the use of smaller channels.

1.3. Supercritical CO_2 power cycles

In line with Gen3 programme recommendations, supercritical CO_2 power cycles are adopted in this study, as they exhibit high thermal efficiency (around 50%) even when the turbine inlet temperature is

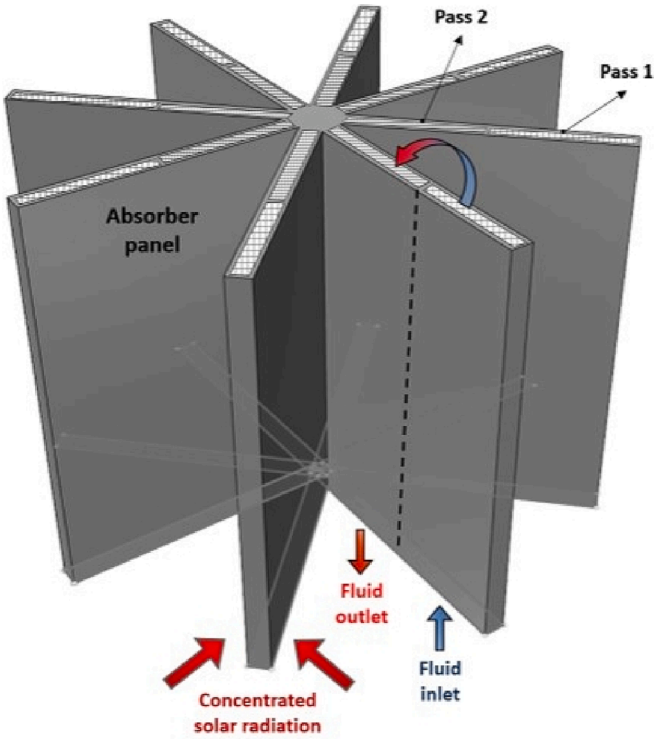

Fig. 2. Scheme of the microchannel central solar receiver analysed in this work.

moderate (around 700 °C). This is because supercritical CO_2 conditions at the compressor inlet are close to the critical point (7.38 MPa, 31 °C), and thus, the CO_2 density is high, so the required compression power is reduced [32].

A comparative study of different sCO_2 cycles indirectly coupled to a molten salt central receiver system, is accomplished in [8]. In that study, several comparative parameters have been weighed, highlighting: the cycle efficiency; the complexity of the cycle, in terms of additional components compared to the most conventional one, the recompression cycle; and the temperature difference in the primary heat exchanger. For a target temperature of 700 °C at the solar receiver outlet, the intercooling cycle exhibits the highest efficiency, followed by the recompression cycle; the simplest layout is the recompression, while the most complex are the intercooling and the partial-cooling, with two extra compressors and an extra intercooler; at last, partial-cooling cycle presents the largest temperature difference in the primary heat exchanger,

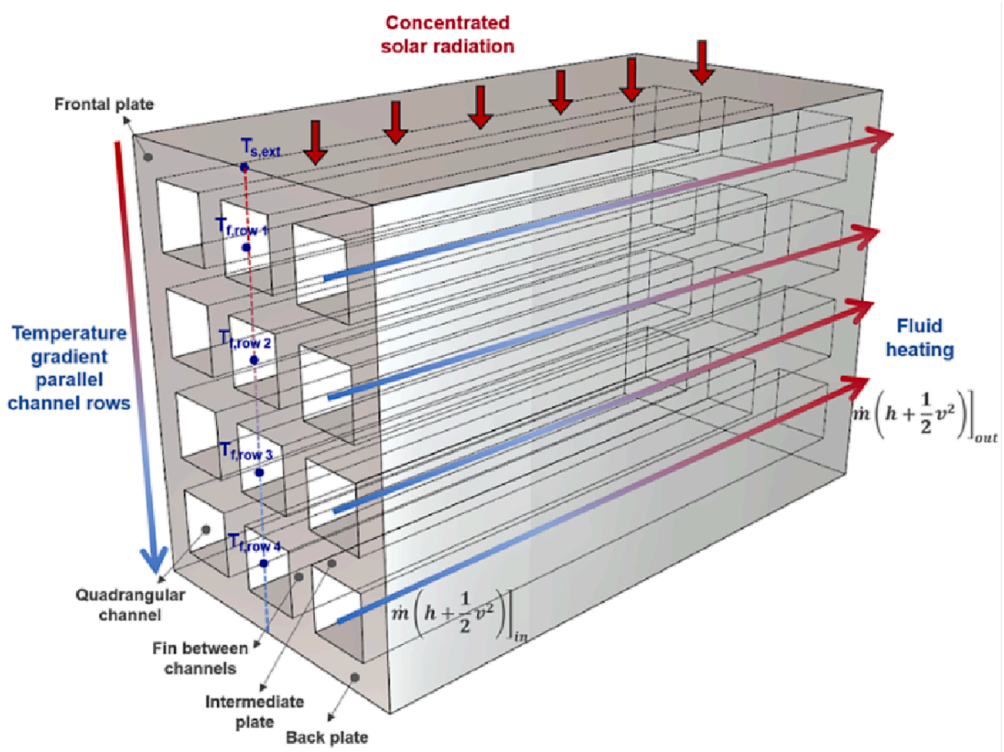

Fig. 3. Thermal resistance circuit to model the heat transfer in the compact structure of the absorber panel.

which in turns reduce the molten salt inventory and the working temperature in the solar receiver, both effects enhancing the STPP performance. A more specific comparative analysis between the recompression and.

partial-cooling sCO_2 cycles is accomplished in [33]. This study concludes that, while the recompression cycle is less complex and it has higher efficiency, the STPP based on the partial-cooling cycle produces more annual electricity and presents lower investment costs because the larger temperature difference in the primary heat exchanger, which reduces both the storage tanks volume and the required pumping power, and it increases the receiver efficiency by a heat losses reduction.

For this comparative study, four sCO_2 cycles have been selected, all based on the recompression configuration: conventional recompression (Fig. 4a), intercooling (Fig. 5a) and.

partial-cooling (Fig. 6a). Finally, for the direct coupling, a new sCO_2 recompression cycle layout is illustrated in Fig. 7a, in which the CO_2 pressure in the thermal supply side of the cycle is lower than the pressures in conventional recompression cycles (85 bar compared to 200–250 bar). The possibility of solarising the sCO_2 cycle at a lower pressure represents a significant advantage and a technical advancement for the feasibility of such configurations. This new layout has already been analysed in previous works [34] and it will be explained in detail in section 2.

1.4. Paper scope and structure

This work addresses the comparative thermo-economic study of different configurations of solar thermal power plants, based on supercritical power cycles and pressurised central receiver systems. To achieve this objective, this manuscript is organised as follows. The methodology section presents all the simulation models used in this study, as well as the value of the main parameters characterising each element of the STPP, specifically the microchannel receiver, the sCO_2 cycles and the heliostat field. As the comparative study focused on nominal conditions, a TES system has not been included in the analysis. However, it is acknowledged that the inclusion of a TES is crucial for assessing the annual performance of the STPP. In the last point of the methodology, it is presented a description of the objective functions for the thermo-economic optimisation. In the results section, the outcomes of several analyses are presented. Firstly, the thermal performance optimisation is discussed in relation to the working fluid conditions in the receiver, specifically temperature and pressure. Secondly, it is examined the effect of different fluids on the thermal performance of the solar subsystem. Lastly, an economic analysis is conducted, which assesses the cost-effectiveness and viability of the studied configurations.

2. Methodology

2.1. Thermal model of the microchannel receiver

As mentioned in the introduction, the selected microchannel receiver is arranged in a radial configuration of the absorber panels, each of them presents an increasing compactness of one pass compared to the previous one, as shown in Fig. 2.

The fluid flows through the absorber panel in two passes, entering through the bottom side of the panel, close to the outer perimeter of the tower, and exiting through the bottom side of the panel close to the tower axis. The compact geometry consists of a plain rectangular fin core, so the channels have a quadrangular section. The receiver material is Alloy 617, which is recommended for compact heat exchangers at the temperatures at which the solar receiver operates [24]. Table 1 shows the main geometrical parameters of the microchannel receiver, that have been optimised for the working temperature range required by the sCO_2 power cycles [30,31]. In this way, the optimal number of absorber panels is eight and their dimensions depend on the HTF and its working conditions; in this work, three HTFs have been considered: CO_2, N_2 and He, although most of the comparative studies in the results section consider CO_2 as the HTF, as the solar subsystem performance is better when using this fluid. It is also observed that the channel dimensions are reduced in pass 2 compared to pass 1, thus increasing compactness and fluid velocity. These values are the result of an optimisation analysis in the working range of the pressurised receivers considered in this work

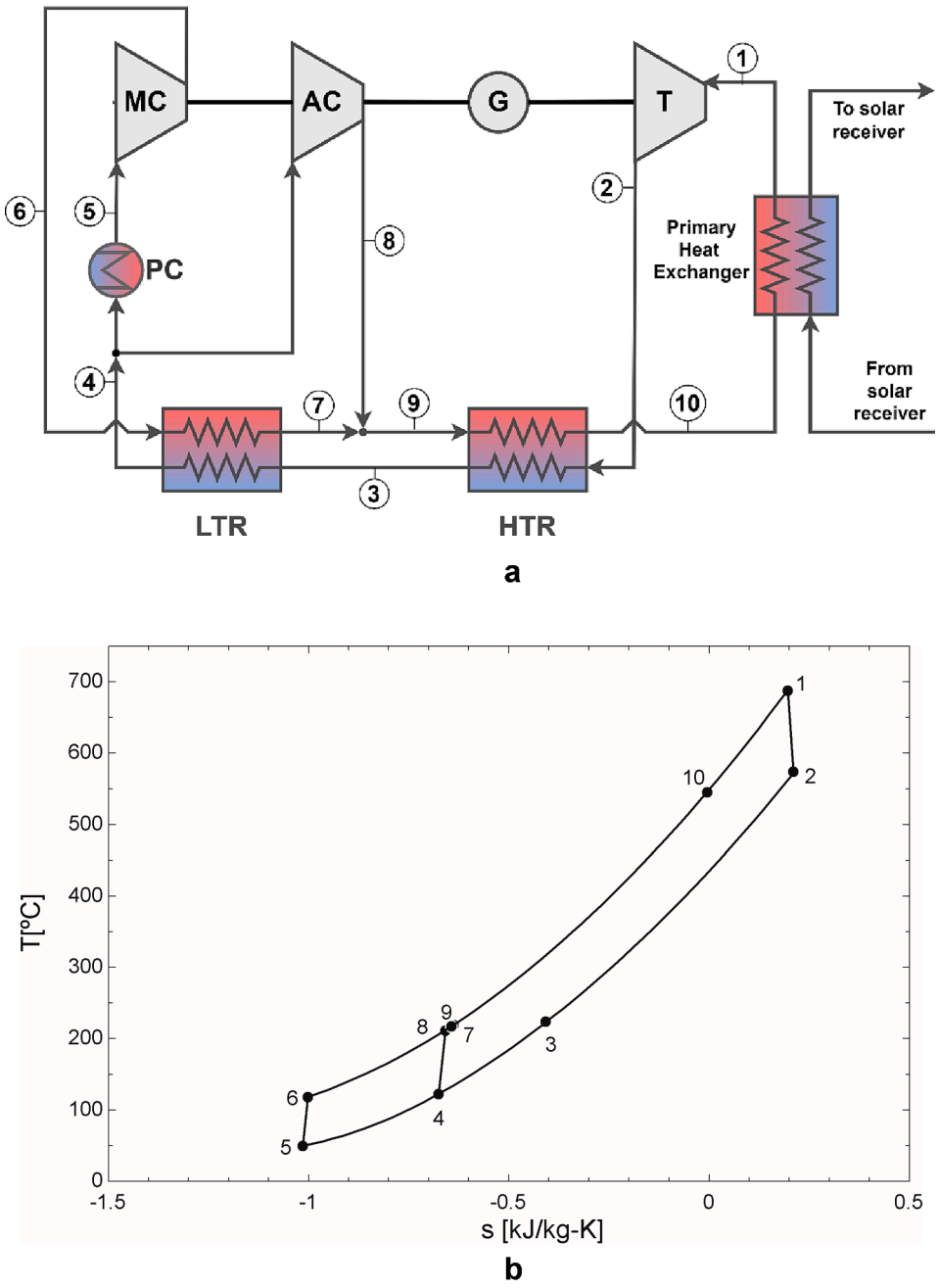

Fig. 4. Supercritical CO_2 recompression cycle, indirect coupling configuration. (a) Layout (b) T-s diagram.

[30,31]. At last, intermediate plate thickness, frontal and back plate thickness, and fin thickness between channels are kept the same in both passes. These geometrical parameters are depicted in Fig. 3.

The receiver thermal model is based on a Thermal Resistance Model (TRM) that characterises the fluid heating along the flow direction. To determine the heat loss, it is necessary to calculate the absorber external surface temperature, for which an additional model is needed to characterise the heat transfer through the panel thickness, between parallel channels rows. Both models have been implemented in Matlab [35], and they have been explained and validated in [36]. Fig. 3 shows schematically the application of the two TRMs to characterise the receiver.

2.2. Thermal model for the sCO_2 power cycle

As said in the introduction, four different sCO_2 cycles have been selected, three of them for a indirectly coupling: conventional recompression, intercooling, and partial-cooling cycles; and the last one for a direct coupling: recompression sCO_2 cycle with solar thermal power supply through the low-pressure side. These supercritical cycles are shown in Fig. 4, Fig. 5, Fig. 6 and Fig. 7, respectively, both the layouts and the temperature – entropy (T-s) diagrams.

The four cycles are based on the recompression layout, so two compressors are included: the main compressor (MC), that supplies the most pressurised stream to the Low Temperature Recuperator (LTR); and the auxiliary compressor (AC), that connects to the High Temperature Recuperator (HTR). The partial-cooling and intercooling cycles differ from the conventional recompression cycle in that the main compressor is split into two (MC1 and MC2) with an intercooling between them. The intercooling and the partial-cooling layouts present different AC inlet conditions as seen in Fig. 5a and Fig. 6a. This difference yields to larger temperature increment of the sCO_2 in the primary heat exchanger of the partial-cooling cycle, which is advisable for the

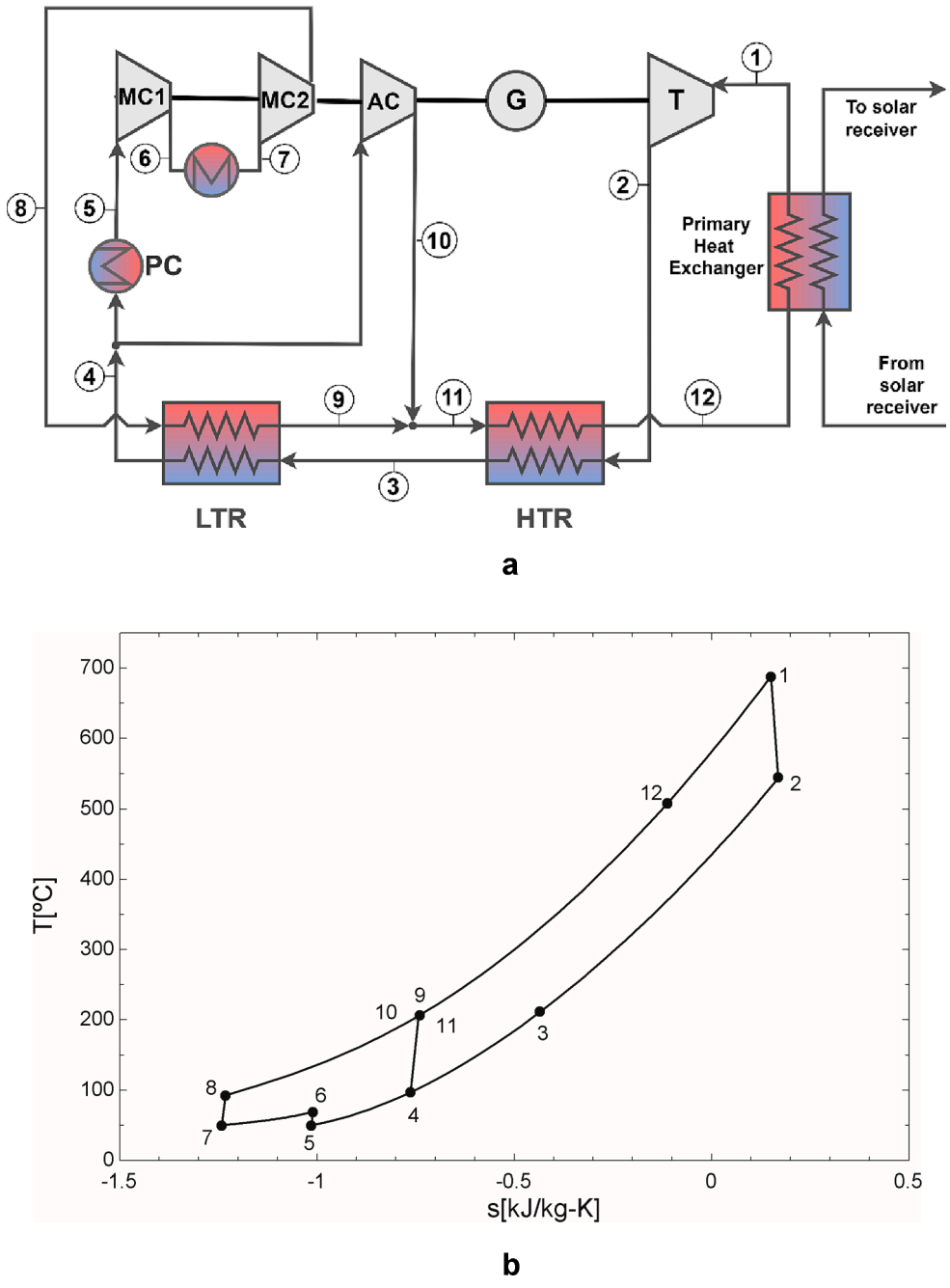

Fig. 5. Supercritical CO_2 intercooling cycle, indirect coupling configuration. (a) Layout (b) T-s diagram.

STPPs, as explained in the introduction. At last, the intercooling cycle achieves a decrease in the compression work that yields to a higher thermal efficiency than the recompression and partial-cooling layouts.

The three indirectly coupled cycles include a PCHE performing as the primary heat exchanger, located upstream the turbine (T), in the high-pressure side of the sCO_2 cycle. The directly coupled cycle differs from the indirect ones in the position in which the solar thermal power is supplied; this is located downstream the turbine in the low-pressure side of the cycle where CO_2 pressure is much lower than in a conventional recompression cycle (85 bar compared to 200 bar).

For all the cycles, the power output has been set to 50 MW_e, which is considered representative of a commercial plant based on this technology [37]. The maximum pressure drop of the sCO_2 in the recuperators has been set at 0.4 bar [38]. The isentropic efficiencies of both the turbine and the compressors have been set at 92% and 88%, respectively, and the mass flow rate split between MC and AC has been set to balance the LTR [34]. Besides, all the cycles present a dry cooling by means of an air-cooled Pre-Cooler (PC).

Table 2 shows the thermodynamic properties of the state points following the numbering marked in Fig. 4a (recompression), Fig. 5a (intercooling), Fig. 6a (partial-cooling) and Fig. 7a (recompression with thermal power supply through the low-pressure side). The fluid temperatures at the inlet / outlet of the solar thermal supply, both in the indirect and direct couplig, are marked in grey.

The sCO_2 thermodynamic properties have been tabulated from NIST database [39] in the working region of the receiver, for temperature steps below 0.4 °C and pressure steps equal to 0.05 bar. As observed in Table 2, the cold source temperature is set at 50 °C, which corresponds to dry-cooling. The numbers highlighted in grey represent the temperatures of the supercritical CO_2 at the inlet and outlet of the primary heat

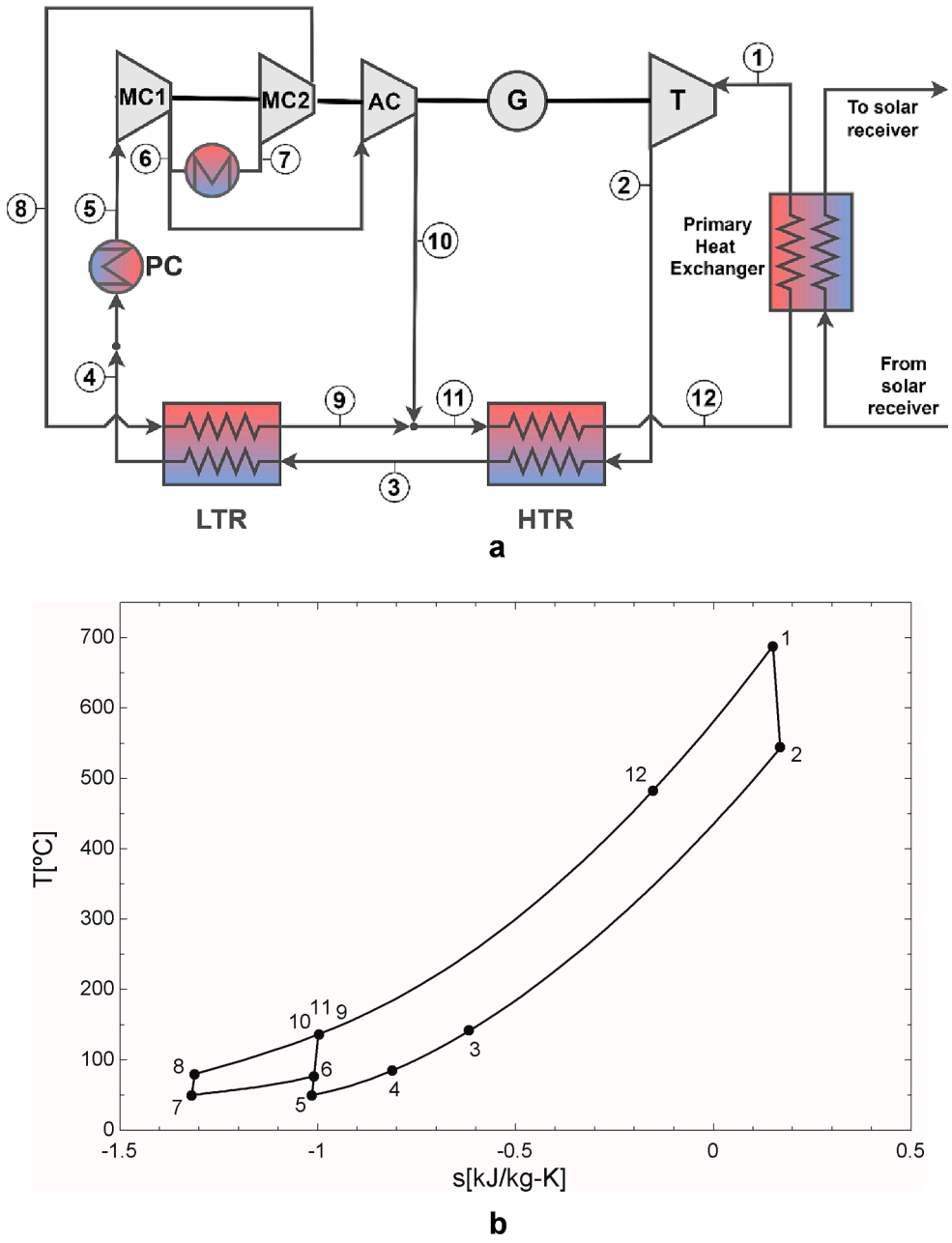

Fig. 6. Supercritical CO_2 partial-cooling cycle, indirect coupling configuration. (a) Layout (b) T-s diagram.

exchanger for the indirectly coupled cycles. It is assumed that the inlet and outlet temperatures of the solar subsystem are 12 °C higher, considering a balanced heat exchanger [5]. In the case of the directly coupled cycle, the temperatures marked in grey directly represent the inlet and outlet temperatures of the solar subsystem.

The main global parameters of each sCO_2 cycle are summarised in Table 3.

As observed in Table 3, the gross power is equal to 50 MW_e for all cycles. This value represents the power supplied by the turbine minus the power consumed by all the compressors included in the cycle. The gross cycle efficiency is defined in Eq. (1) as the ratio between this power ($\dot{W}_{cycle}$) and the solar thermal power ($\dot{Q}_{th,receiver}$), transferred to the CO_2, directly from the microchannel solar receiver, or by means of the primary heat exchanger in indirect coupling.

$$\eta_{gross,cycle} = \frac{\dot{W}_{cycle}}{\dot{Q}_{th,receiver}} = \frac{\dot{W}_T - \dot{W}_C}{\dot{Q}_{th,receiver}} \quad (1)$$

To calculate the net cycle efficiency, internal consumptions have been deducted, including the fan power in the precooler, the intercooler (in the case of cycles with partial-cooling or intercooling), as well as the power consumed by the blower that drives the CO_2 through the solar subsystem. The power consumed by this blower depends on the pressure drop of the fluid through the receiver, and this value, in turn, depends on the working pressure in the solar loop. In the case of direct coupling, this pressure is fixed by the cycle, while in other cases, the power consumed by the blower has been calculated for the working pressure that optimises the exergy efficiency of both the heliostat field and receiver, as will be seen in the results section: 85 bar for conventional recompression; 65 bar for intercooling; and 55 bar for partial-cooling. The efficiency of this blower has been assumed to be 70%. Once the above values are defined, the net efficiency is calculated according to the following Eq. (2).

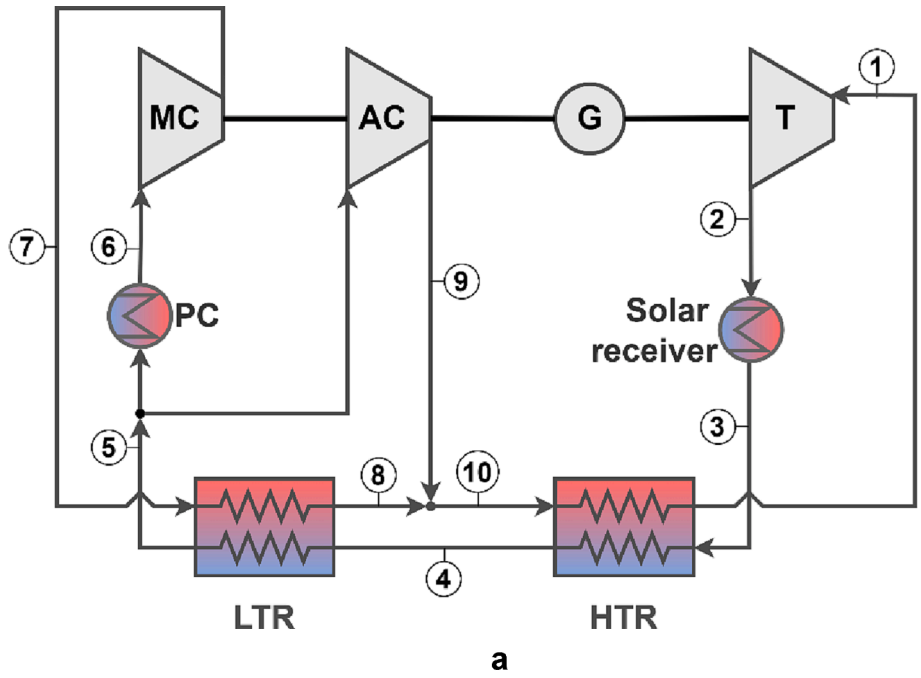

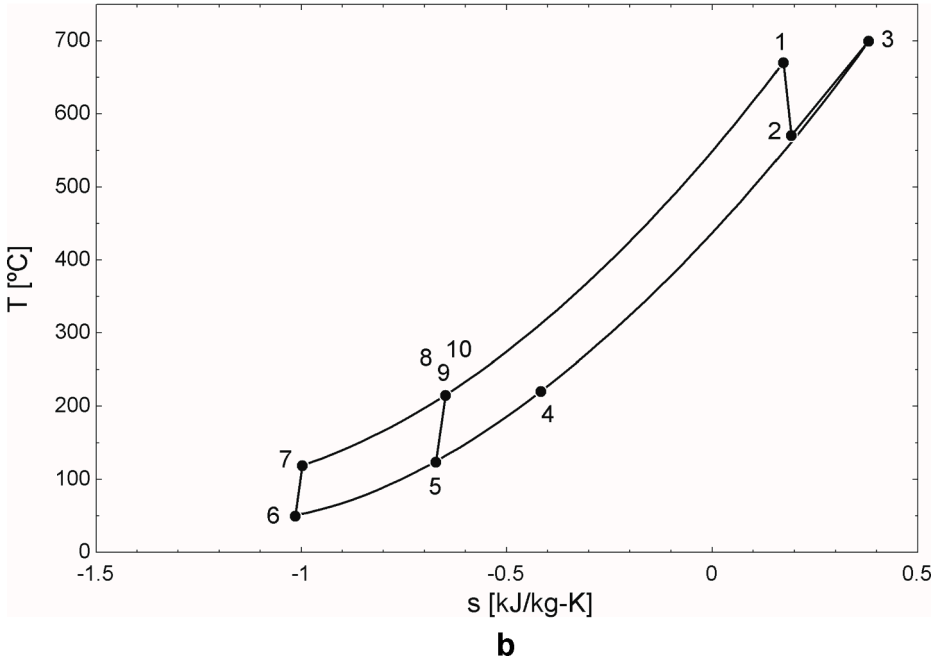

Fig. 7. Supercritical CO2 recompression cycle with solar thermal power supply through the low-pressure side, direct coupling configuration (Source: [30]). (a) Layout (b) T-s diagram.

$$\eta_{net,cycle} = \frac{\dot{W}_{cycle} - \dot{W}_{fans} - \dot{W}_{blower}}{\dot{Q}_{th,receiver}} \quad (2)$$

2.3. Optical model for the solar field subsystem

The heliostats are arranged in a circular solar field, and they concentrate the sunlight on the receiver located at the top of the tower. The tower height is calculated by means of the equation shown in Table 4, as function of the receiver thermal power [40]. It is important to note that, although the tower height is apparently small compared to current commercial plants, it is within the limits given in [41], and in accordance with the default heliostat size used by the SolarPilot software [42]. Based on the thermal power, the absorber panel dimensions are also calculated, keeping the geometrical parameters listed in Table 1, which are optimal for the thermal power range and working conditions used in this comparative analysis [30,31].

The tower height, thermal power and receiver sizing, together with the design point conditions shown in Table 4, are introduced in SolarPilot to calculate the circular heliostat field. The heliostat characteristics as well as the optical errors are the default ones in SolarPilot, also shown in Table 4. This heliostat field is then exported to Soltrace software [43], to perform a Monte Carlo ray tracing and to calculate more accurately the optical efficiency and the solar flux map on each of the absorber panels. All calculations obtained refer to nominal conditions of the sCO_2

Table 1
Themo-fluid and geometrical parameters of the receiver.

Global characteristics of the absorber panel	
Number of absorber panels	8
Material	Inconel 617
Aspect Ratio	0.7
Number of flow passes in the panel	2
Compact structure	Plain rectangular fin
Channel shape	Quadrangular
Pass 1	
Channel dimensions in pass 1 (mm × mm)	12 × 12
Number of channel rows in pass 1	6
Plate thickness (mm)	1
Frontal / back plate thickness (mm)	1.5
Thickness between channels (mm)	3
Average fluid velocity ($m{\cdot}s^{-1}$)	15
Pass 2	
Channel Dimensions (mm × mm)	5 × 5
Number of channel rows	6
Plate thickness (mm)	1
Frontal / back plate thickness (mm)	1.5
Thickness between channels (mm)	3
Average fluid velocity ($m{\cdot}s^{-1}$)	30

cycle and the design point of the solar field. The number of heliostats depends on each specific case, and it has been calculated for each of the cases analysed in the results section.

2.4. Description of the comparative analysis and objective functions for the thermo-economic optimisation

The first objective of the comparative study was to analyse several working conditions of the heat transfer fluid (HTF) in the solar receiver, specifically focusing on CO_2 for the initial analysis. The investigation aimed to assess the impact of CO_2 pressure at the receiver inlet for the cycles with indirect coupling (recompression, intercooling, partial-cooling). The objective functions for this comparative analysis have been the energy and exergy efficiencies, including the heliostat field and the solar receiver, Eq. (3) and Eq. (4):

$$\eta_{en,\ solar\_field\ \&\ receiver} = \eta_{opt}{\cdot}\eta_{en,\ receiver} \tag{3}$$

$$\eta_{ex,\ solar\_field\ \&\ receiver} = \eta_{opt}{\cdot}\eta_{ex,receiver} \tag{4}$$

Eqs. (3) and (4) include the heliostat field optical efficiency, η_{opt}, calculated by means of Soltrace [43], and the receiver energy and exergy efficiencies, calculated using the simulation model [25,26]. These efficiencies are given by Eq. (5) and Eq. (6), respectively.

$$\eta_{en,receiver} = \frac{\dot{Q}_{th,HTF,receiver}}{\dot{Q}_{solar,receiver}} \tag{5}$$

$$\eta_{ex,receiver} = \frac{\Delta Ex_{HTF,receiver}}{\Delta Ex_{solar,receiver}} \tag{6}$$

In the above equations, $\dot{Q}_{th,HTF,receiver}$ is the thermal gain of the HTF through the receiver, calculated by Eq. (7); $\Delta Ex_{HTF,receiver}$ is the exergy gain of the HTF; as the HTF working conditions in the receiver are far enough from the critical point, ideal gas with constant specific heats behaviour is assumed, so the exergy gain is given by Eq. (8); $\dot{Q}_{solar,receiver}$ is the concentrated solar radiation on the receiver, while $\Delta Ex_{solar,receiver}$ is the exergy of this incident solar radiation, calculated by Parrot equation [44], Eq. (9).

$$\dot{Q}_{th,HTF,receiver} = \dot{m}\left[(h_{out} - h_{in}) + \frac{1}{2}\left(v_{out}^2 - v_{in}^2\right)\right] \tag{7}$$

$$\Delta Ex_{HTF,receiver} = \dot{m}\left[\Delta h\left(1 - \frac{T_{amb}}{T_{lm}}\right) + RT_{amb}\ln\left(\frac{P_{out}}{P_{in}}\right)\right] \tag{8}$$

$$\Delta Ex_{solar,receiver} = \dot{Q}_{solar,receiver}{\cdot}\left[1 - \frac{4}{3}{\cdot}\frac{T_0}{T_s}{\cdot}(1-\cos\delta)^{1/4} + \frac{1}{3}{\cdot}\left(\frac{T_0}{T_s}\right)\right] \tag{9}$$

In the above equations, $\dot{m}$ is the fluid mass flow through the receiver; h is the fluid enthalpy at the inlet / outlet of each receiver element; v is the fluid velocity at the inlet / outlet of each receiver element; T_{amb} is the ambient temperature; T_{lm} is the log mean fluid temperature at the inlet / outlet of each receiver element, defined as $T_{lm} = \frac{T_{in}-T_{out}}{ln(T_{in}/T_{out})}$; R is the ideal gas constant; P is the fluid pressure, evaluated at the inlet / outlet of each receiver element; T_0 is the reference temperature, equal to the ambient temperature; T_s is the equivalent temperature of the sun as a blackbody (~5800 K); and δ is the half–angle of the cone subtended by the sun's disc ($\delta \sim 0.0047$ rad, on a clear day).

In the study of each STPP using indirect coupling, it was determined the optimal CO_2 pressure that maximises the performance of the sub-system including the solar field and the receiver. For each optimal case identified, the overall STPP efficiency was calculated and compared to the case of direct coupling, where the receiver input conditions were kept constant. The overall STPP efficiency is defined according to Eq. (10):

$$\eta_{overall,\ STPP} = \eta_{opt}{\cdot}\eta_{en,\ receiver}{\cdot}\eta_{net,cycle} \tag{10}$$

Table 2
Thermodynamic properties of the state points of each sCO_2 cycle.

	Recompression cycle				Intercooling cycle				Partial-cooling cycle				Direct coupling cycle			
	P (bar)	T (ºC)	h (kJ/kg)	s (kJ/kg/K)	P (bar)	T (ºC)	h (kJ/kg)	s (kJ/kg/K)	P (bar)	T (ºC)	h (kJ/kg)	s (kJ/kg/K)	P (bar)	T (ºC)	h (kJ/kg)	s (kJ/kg/K)
1	200	688	701.3	0.20	250	688	699.5	0.15	250	688	699.5	0.15	200	670.5	679.1	0.17
2	86.2	574.1	566.5	0.21	86.2	545.1	531.4	0.17	86.2	545.1	531.4	0.17	89.87	567.7	558.5	0.19
3	85.8	224.2	158.4	-0.41	85.8	212.3	144.9	-0.44	85.8	142.3	62.99	-0.62	86.2	700	721.3	0.38
4	85.4	122.9	39.09	-0.68	85.4	97.71	5.775	-0.76	85.4	85.38	-12.13	-0.81	85.8	220.5	154.3	-0.42
5	85	50	-80.9	-1.02	85	50	-80.9	-1.02	85	50	-80.9	-1.02	85.4	124	40.57	-0.67
6	201.2	118.3	-41.57	-1.00	108.5	68.92	-71.05	-1.01	120.3	77.05	-66.64	-1.01	85	50	-80.9	-1.02
7	200.8	219.6	117.4	-0.64	108.1	50	-147.6	-1.24	119.9	50	-170.2	-1.32	200.8	119	-39.81	-1.00
8	200.8	212	107.2	-0.66	251.2	92.71	-118.9	-1.23	251.2	80.18	-147.1	-1.31	200.4	215.5	112.1	-0.65
9	200.8	217.7	114.9	-0.64	250.8	207.3	86.56	-0.74	250.8	137.1	-26.99	-1.00	200.4	215.5	112.1	-0.65
10	200.4	545.6	522.9	-0.01	250.8	205.8	84.32	-0.74	250.8	136.3	-28.48	-1.00	200.4	215.5	112.1	-0.65
11					250.8	206.8	85.84	-0.74	250.8	136.8	-27.54	-1.00				
12					250.4	508	472.4	-0.11	250.4	482.8	440.9	-0.15				

Table 3
Main global parameters of each sCO_2 cycle.

	Recompression cycle	Intercooling cycle	Partial-cooling cycle	Direct coupling cycle
Cycle gross power (MW_e)	50	50	50	50
Precooler fan power consumption (kW_e)	291.7	143.9	157.2	380.1
Intercooling fan power consumption (kW_e)	–	127.1	148.1	–
Solar subsystem blower power consumption (kW_e)	8463	6554	6780	–
Source thermal power (MW_{th})	101.031	97.35	103.36	116.45
Cycle gross efficiency (%)	49.49	51.36	48.37	42.94
Cycle net efficiency (%)	40.82	44.35	41.52	42.61

Table 4
Parameters for the heliostat field calculation. .

Design point conditions	
Location (latitude, longitude)	Seville (37.4 N, 5.9 W)
Day and hour	21st March, solar noon
Direct Normal Irradiation, DNI (W m^{-2})	950
Ambient temperature (°C)	25
Effective sky temperature (°C)	15
Wind velocity (m s^{-1})	2
Tower height	
$H_{tower} = 0.2552 \cdot \dot{Q}_{th,receiver}(MW_{th}) + 82.6$[40,41]	
Heliostat geometry and focusing	
Structure width (m) × height (m)	12.2 × 12.2
N. of horizontal panels	2
N. of vertical panels	8
Optical error parameters	
Elevation pointing error (rad)	0
Azimuth pointing error (rad)	0
Surface slope error in X / Y (mrad)	1.53
Reflected beam error in X / Y (mrad)	0.2
Mirror performance parameters	
Reflective surface ratio	0.97
Mirror reflectivity	0.95
Soiling factor	0.95

Source: [40,41,42]

A second comparative study has been conducted to analyse the performance of different HTFs in the solar receiver, specifically focusing on CO_2, N_2 or He. In this analysis, the energy efficiency and exergy efficiency, calculated using equations (3) and (4) respectively, have been considered as objective functions.

At last, a comparative economic analysis has been conducted for each optimum indirectly coupled configuration – adopting the CO_2 pressure at the receiver inlet that maximises the exergy efficiency- and the directly coupled configuration. For this analysis, the Total Capital Cost (TCC) [45] and the Levelised Cost of Energy (LCOE) [46,47] of each STPP have been estimated.

The LCOE is calculated by means of the investment cost and the annual electricity production of the STPP, using the following Eq. (11) and Eq. (12):

$$LCOE = \frac{CRF \cdot TCC}{AEP} + OMC \tag{11}$$

$$CRF = \frac{WACC \cdot (1 + WACC)^n}{(1 + WACC)^n - 1} \tag{12}$$

In Eq. (11), CRF (%) is the Capital Recovery Factor; TCC ($) is the total capital cost of the STPP (power cycle and solar subsystem); AEP (kWh_e) is the Annual Electricity Production by the STPP, taking into account that stand-alone CSP plants operate with reduced capacity factors (CF), in the range of 22–28% [48,49]; OMC is the O&M costs per kWh, taken from [1,50]; by using directly OMC, it is assuming that the O&M nominal escalation rate is null and thus, the Constant Escalation Levelisation Factor (CELF) is equal to 1. Finally, in Eq. (12), WACC is the Weighted Average Capital Cost.

3. Results and discussion

3.1. Optimisation of the solar subsystem thermal performance as function of the working conditions of the CO_2 at the inlet of the solar receiver.

This first analysis is limited to STPP configurations with indirect coupling to a sCO_2 cycle, specifically considering conventional recompression, intercooling, or partial-cooling options. The study does not encompass the direct coupling case since the working conditions in that configuration are imposed by the power cycle. However, a comparison between the direct coupling and the optimum of each of the other configurations is addressed at the end of this section.

For each indirectly coupled configuration, the solar subsystem performance has been assessed, including both the optical efficiency of the heliostat field and the receiver energy and exergy efficiencies, as function of the HTF working conditions in the solar receiver, yielding to the results shown in Fig. 8 (recompression), Fig. 9 (intercooling) and Fig. 10 (partial-cooling). The HTF in the solar receiver is CO_2, since, as will be demonstrated in section 3.2, it has good thermal properties in the working range of the pressurised receiver. The CO_2 pressure at the solar receiver inlet has been evaluated, within 25 bar and 85 bar, as displayed on the abscissa axis in Fig. 8, Fig. 9, and Fig. 10. As the pressure increases, the absorber panel dimensions decrease, as shown in Table 5.

The effect of CO_2 temperature in the solar subsystem has been analysed by coupling to the different sCO_2 cycles described in section 2.2, and assuming that the primary heat exchanger between the solar subsystem and the power cycle is balanced with a temperature difference of.

12 °C [5]. For these conditions, the thermal increment in the solar receiver can be estimated as follows: 557.6 °C to 700 °C for conventional recompression; 520 °C−700 °C for intercooling; 494.8 °C to 700 °C for partial-cooling. That is, the average working temperature is highest for recompression (628.8 °C), followed by the intercooling (610 °C) and finally, partial-cooling (597.4 °C). This temperature has an important effect on the solar subsystem performance, as it is a key factor in achieving optimum energy and exergy efficiency; as can be seen in the previous figures, the maximum energy and exergy efficiencies occur for a CO_2 pressure of 55 bar in the partial-cooling case (Fig. 10), 65 bar in the intercooling case (Fig. 9) and there is no maximum for conventional recompression case (Fig. 8), in the working pressure range analysed. This latter trend is caused because, as the operating temperature increases, the heat losses increase, being therefore the highest for the receiver coupled to the recompression cycle, as shown in Table 5; thus, for this latter configuration, the receiver size reduction as the pressure increases is always beneficial, even if the optical efficiency decreases.

The effect of the solar receiver size for a given pressure is explained as follows: the absorber panel dimensions are slightly larger as the average CO_2 temperature in the receiver increases; that is, for a given pressure, the receiver coupled to the recompression cycle is slightly larger than that coupled to the intercooling cycle, the smallest being that coupled to the partial-cooling cycle. This effect is explained because heat transfer is worse as the fluid temperature increases, so more surface area is needed to reach the target temperature of 700 °C. The receiver size affects the optical efficiency, which decreases as the dimensions of the

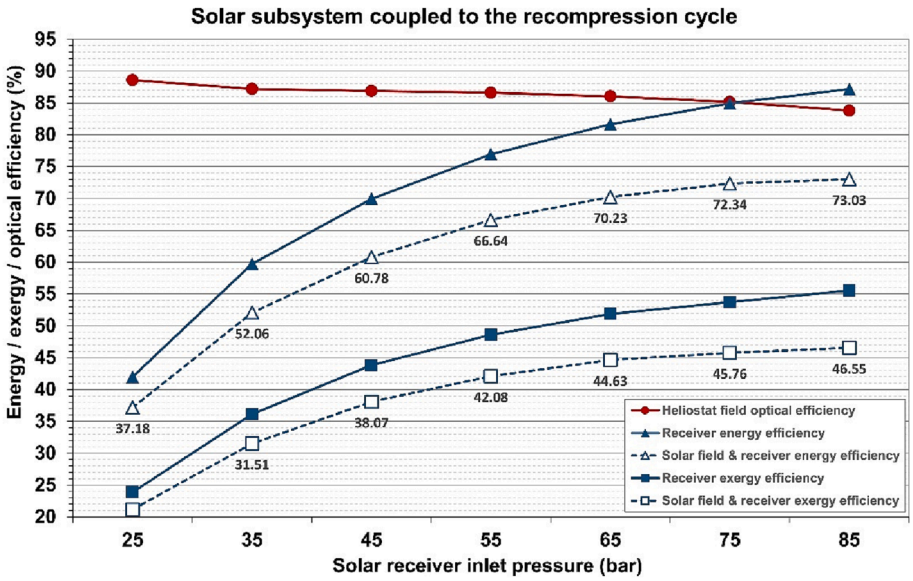

Fig. 8. Optical and thermal performance of the solar subsystem coupled to the conventional recompression sCO_2 cycle.

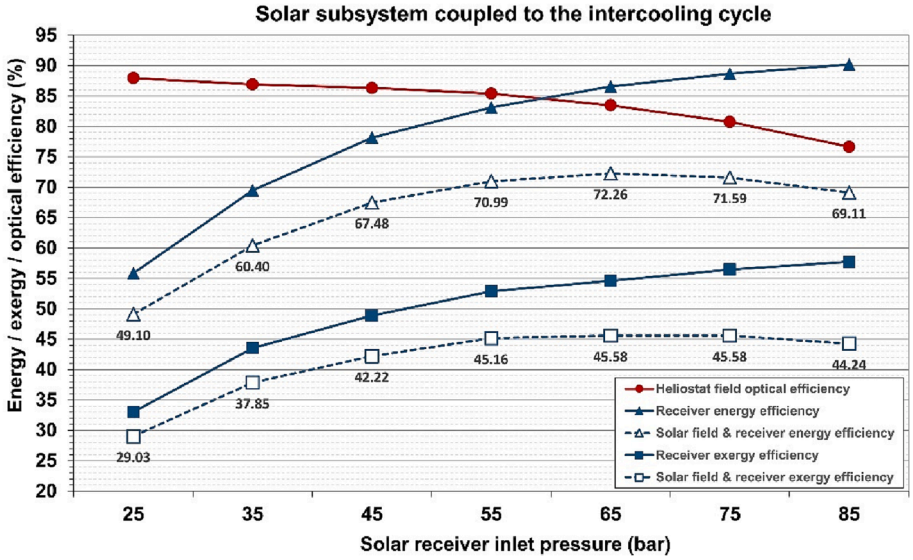

Fig. 9. Optical and thermal performance of the solar subsystem coupled to the intercooling sCO_2 cycle.

absorber panel are reduced; therefore, the net decrease of the optical efficiency in the working pressure range considered is lower for the recompression case (Fig. 8) than for the intercooling or partial-cooling cases (Fig. 9 and.

Fig. 10, respectively). The receiver size also affects its energy and exergy efficiency. The net increase of both efficiencies in the working pressure range considered is higher in case of higher working temperature (recompression case, Fig. 8), as the heat losses per unit area are also higher, therefore a reduction of the exposure area has a higher positive impact on the receiver thermal performance.

Finally, Table 6 shows the values of the main parameters that define the performance of each of the optimal STPP configurations previously calculated, together with the configuration corresponding to the direct coupling to the sCO_2 recompression cycle with thermal power supply through the low-pressure side. In this case, only one set of working conditions has been considered (receiver inlet pressure of 86.6 bar and a thermal increment between 510 °C and 700 °C in the receiver). Although it is possible to modify the operating conditions in the solar subsystem by incorporating new elements in the global scheme, any modification of these conditions will also affect the power cycle performance, which complicates the optimisation process and requires a more extensive study, beyond the scope of this work.

As seen in Table 6, for the indirect coupling option and the working conditions previously indicated, the STPP with the highest overall efficiency is the one based on the intercooling sCO_2 cycle, followed by the conventional recompression and, finally, the partial-cooling cycle. This is due to the intercooling cycle exhibiting the highest net efficiency among the indirectly coupled configurations. Additionally, the solar subsystem efficiency is also high in this case, primarily because of the low inlet temperature and the large temperature increment in the primary heat exchanger. These values fall between those observed in the recompression and partial-cooling options.

It is also important to note that the STPP based on the novel proposal of directly coupled recompression cycle is only comparable to the configuration based on the indirectly coupled conventional recompression cycle, resulting a better performance in the latter compared to the former because, although the cycle efficiency is higher in the direct coupling option, the solar subsystem performance is favoured by the

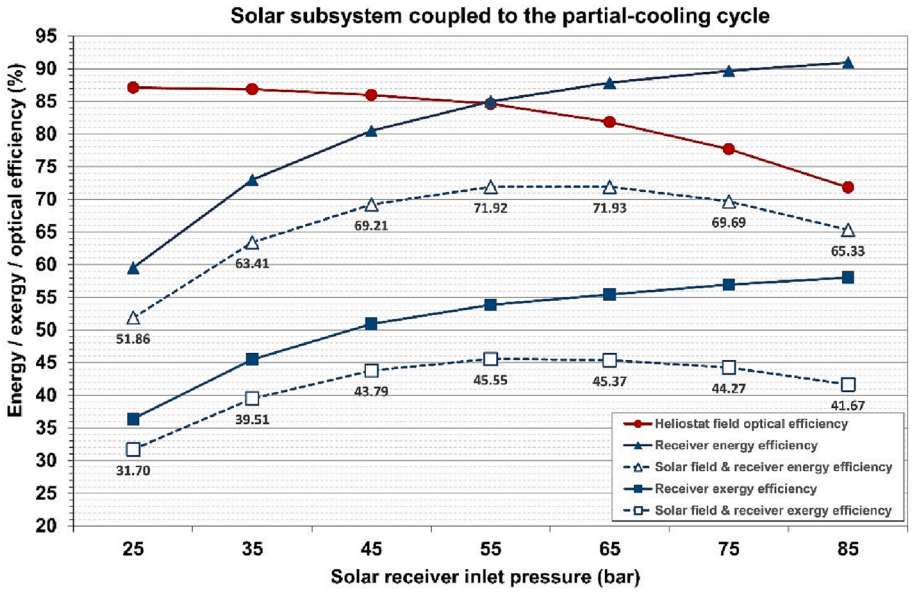

Fig. 10. Optical and thermal performance of the solar subsystem coupled to the partial-cooling sCO_2 cycle.

Table 5

Panel dimensions, heat loss, pressure drop in the solar receiver indirectly coupled to each $sCCRF = \frac{WACC \cdot (1+WACC)^n}{(1+WACC)^n - 1}$ O_2 recompression layout, as function of the CO_2 pressure at the solar receiver inlet.

Inlet pressure (bar)	Recompression				Intercooling				Patial-cooling			
	Panel height (m)	Panel width (m)	Heat loss (kW_{th})	ΔP (bar)	Panel height (m)	Panel width (m)	Heat loss (kW_{th})	ΔP (bar)	Panel height (m)	Panel width (m)	Heat loss (kW_{th})	ΔP (bar)
25	20.80	14.86	7782.46	6.17	15.66	11.19	4886.52	4.68	14.45	10.32	4346.27	4.35
35	14.84	10.60	4237.98	5.78	11.18	7.99	2638.79	4.39	10.32	7.37	2377.39	4.07
45	11.54	8.24	2676.14	5.52	8.69	6.21	1707.96	4.19	8.00	5.72	1552.82	3.89
55	9.43	6.74	1878.84	5.33	7.11	5.08	1231.77	4.05	6.55	4.68	1138.27	3.76
65	7.97	5.69	1415.96	5.19	5.99	4.28	954.39	3.93	5.53	3.95	897.39	3.65
75	6.91	4.93	1128.98	5.07	5.19	3.71	782.21	3.84	4.79	3.42	745.38	3.57
85	6.10	4.36	934.95	4.98	4.57	3.26	664.79	3.77	4.22	3.02	644.33	3.49

Table 6

Main parameters defining the performance of the solar thermal power plants analysed, including directly coupled and indirectly coupled configurations.

	Direct coupling	Indirect coupling		
	Recompression with thermal supply in low pressure side	Conventional recompression	Intercooling	Patial-cooling
Receiver panel height (m)	6.71	6.1	5.99	6.55
Receiver panel width (m)	4.79	4.36	4.28	4.68
Receiver heat loss (kWth)	1103.79	934.95	954.39	1138.27
Receiver pressure drop (bar)	5.85	4.98	3.93	3.76
Heliostat field optical efficiency (%)	77.31	83.79	83.48	84.61
Receiver energy efficiency (%)	86.93	87.16	86.56	85
Receiver exergy efficiency (%)	55.12	55.56	54.6	53.84
Cycle net efficiency (%)	42.61	40.82	44.35	41.52
Overall STPP efficiency (%)	28.64	29.81	32.05	29.86

lower inlet temperature and larger temperature increment of the thermal supply in the indirect coupling option. For future works, the directly coupled cycle could also incorporate partial-cooling and intercooling, and these cases should be compared to the corresponding indirectly coupled configurations.

3.2. Effect of the heat transfer fluid on the solar subsystem performance

In the previous section, the HTF in the solar receiver has been assumed to be CO_2. Nevertheless, the type of HTF has a great influence on the receiver sizing and, therefore, on the solar subsystem performance. This section aims to show this effect by performing a comparative analysis between CO_2, N_2 and He in the receiver, for each of the supercritical cycles with indirect coupling and each of the optimum pressures shown in section 3.1. The result of this comparison is shown in Table 7 and Fig. 11.

Fig. 11 shows that the solar subsystem energy and exergy efficiency when using He is lower than with N_2 and, in turn, N_2 is lower than with CO_2, all under the same working conditions of pressure and temperature. The reason for this lower efficiency is the worse heat transfer properties of the He or N_2, compared to CO_2, which means that the receiver dimensions are slightly larger, all other conditions being equal,

Table 7
Panel dimensions, heat loss, pressure drop in the solar receiver indirectly coupled to each sCO_2 cycle, as function of the heat transfer fluid in the solar subsystem (CO_2, N_2 or He).

HTF	Recompression (85 bar at the solar receiver inlet)				Intercooling (65 bar at the solar receiver inlet)				Patial-cooling (55 bar at the solar receiver inlet)			
	Panel height (m)	Panel width (m)	Heat loss (kW_{th})	ΔP (bar)	Panel height (m)	Panel width (m)	Heat loss (kW_{th})	ΔP (bar)	Panel height (m)	Panel width (m)	Heat loss (kW_{th})	ΔP (bar)
CO_2	6.097	4.355	934.948	4.982	5.991	4.279	954.395	3.935	6.549	4.678	1138.270	3.759
N_2	10.336	7.383	2204.406	5.680	10.111	7.222	2213.332	4.501	10.998	7.856	2655.515	4.305
He	15.810	11.293	4535.667	1.921	15.434	11.024	4515.296	1.551	16.771	11.979	5450.463	1.498

as shown in Table 7. These larger dimensions result in higher heat losses in the solar receiver using He, followed by N_2 and, finally, CO_2.

The investment in the solar field is also higher in the case of using He or N_2, compared to CO_2, as the dimensions of the receiver are larger. Although it would be necessary to analyse the cost difference between HTFs, as well as other technological implications related to the operation and maintenance, it seems a priori that the use of CO_2 is more advantageous than the other options.

3.3. Economic analysis

In this last section, a comparative economic analysis has been carried out for the STPP configurations with the highest exergy efficiency of the solar subsystem (calculated in section 3.1), as well as the case of direct coupling to a sCO_2 recompression cycle with thermal power supply through the low-pressure side. For this purpose, it has been estimated the TCC and the LCOE of each configuration.

The solar subsystem TCC has been estimated by means of the SolarPilot software and it mainly includes the total capital cost related to the tower, the receiver and the heliostat field.

Table 8 shows the numerical values of the main parameters, for each STPP configuration. The cost calculation equations are based on a design parameter, namely: the tower height -calculated using equation shown in Table 4-, for the tower cost; the receiver absorber area -calculated by the panels height and width, in Table 5 and Table 6-, for the receiver; and the number of heliostats.

-calculated directly using SolarPilot-, for the heliostat field. Although the tower height is kept almost constant, there are notable differences between the number of heliostats and the receiver area. Thus, the solar subsystem that exhibits the lowest investment cost is the one coupled to the intercooling cycle, due to the lowest values of receiver area and number of heliostats.

The power cycle TCC has been calculated by means of the methodology explained in ([4,30]). This calculation is referred to the primary heat exchanger, the turbomachinery, the recuperators (LTR and HTR) and the precooler. For each item in previous table, the total investment cost includes Purchase Equipment Cost (PEC), the share in pipes, instrumentation and control (118% of PEC) and indirect cost (25% of PEC), according to [44]. The values calculated are shown in Table 9. In this case, the cycle with lowest investment cost is the partial-cooling, followed by the intercooling, the direct coupling and finally, the recompression layout. In this case, the biggest difference is caused by the LTR and HTR recuperators, which are less voluminous in the cases of partial-cooling and intercooling.

The LCOE for each optimised configuration is calculated using Eq. (10) and the values assumed and justified in section 2.4, as summarised in Table 10.

The configuration with the lowest LCOE is the one with the lowest TCC, which in this case is the STPP based on the partial-cooling cycle. Although this configuration has a higher investment cost in the solar subsystem compared to the intercooling configuration, the power cycle investment cost is considerably lower compared to the others, which leads to a lower LCOE. The direct coupling configuration is the second, followed by the STPP based on the intercooling cycle and lastly, the STTP based on the recompression cycle. Although the directly coupled configuration incurs higher investment costs compared to the intercooling configuration, the levelised cost is lower due to the higher electricity production resulting from lower self-consumption (fans and blower). It is important to highlight that the directly coupled configuration does not require a blower in the solar loop, and the CO_2 compression is performed at a lower temperature compared to the options with indirect coupling, so the electricity consumption is lower.

To finish this section, it can be concluded that there are several factors that lead to a reduction of the investment costs in STPPs based on sCO_2 cycle, both in the power block and in the tower system. Concerning the power cycle, configurations in which the number and volume of heat exchangers are reduced should be chosen, as the turbomachinery cost is similar; in this way, the direct coupling configuration has the advantage of not requiring the primary heat exchanger. In addition, a higher cycle efficiency yields to a lower thermal power required and thus to smaller receiver dimensions and number of heliostats. At last, lower average temperature in the primary heat exchanger yields to lower working temperature and heat losses in the solar receiver. Concerning the solar subsystem, it has been proven that working with HTF at high pressure is beneficial, as it reduces the receiver dimensions and the number of heliostats, although there is an optimum pressure for which the exergy efficiency of the solar field is maximum. Beyond this pressure, the number of heliostats required increases, increasing the cost again.

4. Conclusions

This paper presents a comparative thermo-economic study of different STPP schemes based on sCO_2 cycles and pressurised solar central receiver systems. The working fluid in the solar subsystem is a pressurised gas or a supercritical fluid; the receiver consists of absorber panels arranged in a radial configuration, and each panel consists of a compact geometry of plain rectangular fin type. This design has been validated and optimised in previous works. For the comparative study, different sCO_2 layouts have been evaluated, both indirectly coupled (conventional recompression, intercooling and partial-cooling) and directly coupled to the solar subsystem (recompression cycle with thermal supply in the low pressure side). Three possible HTFs have been considered in the solar tower system: CO_2, N_2 and He. For the former, a comparative analysis has been conducted, calculating the energy and exergy efficiency of the solar subsystem as a function of the receiver inlet pressure. Finally, it has been carried out an economic analysis of the STPP configurations optimised in the previous study. The main conclusions obtained from this study are summarised as follows:

- The selection of the sCO_2 cycle affects the overall thermal performance of the STPP. In this way, two factors have been identified that improve the performance of the plant: the power cycle efficiency, since, for the same electrical power, the higher the efficiency, the lower the thermal power required from the solar subsystem, which reduces its size and thus the total investment cost; the temperature increment in the primary heat exchanger, since it reduces the volume of pressurised gas (or supercritical fluid) and thus the solar receiver size, while lowering the working temperature in the solar receiver and, therefore, the heat losses.

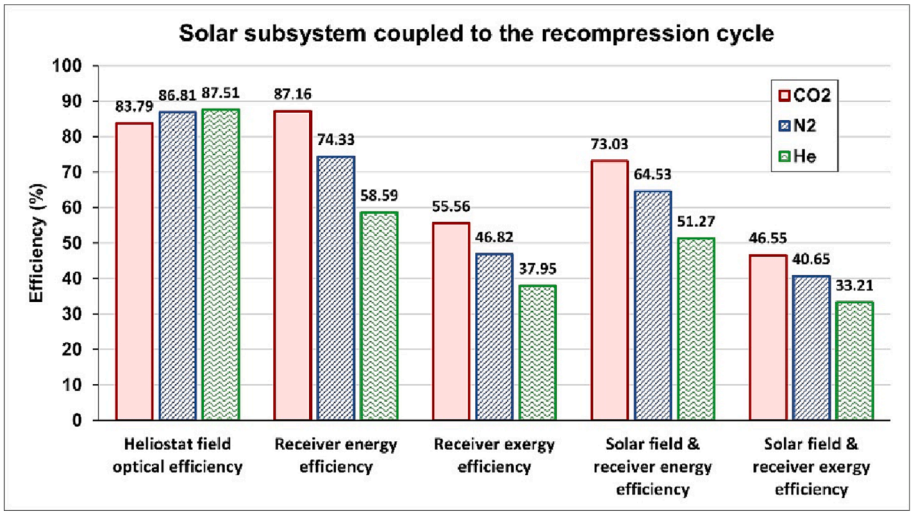

a

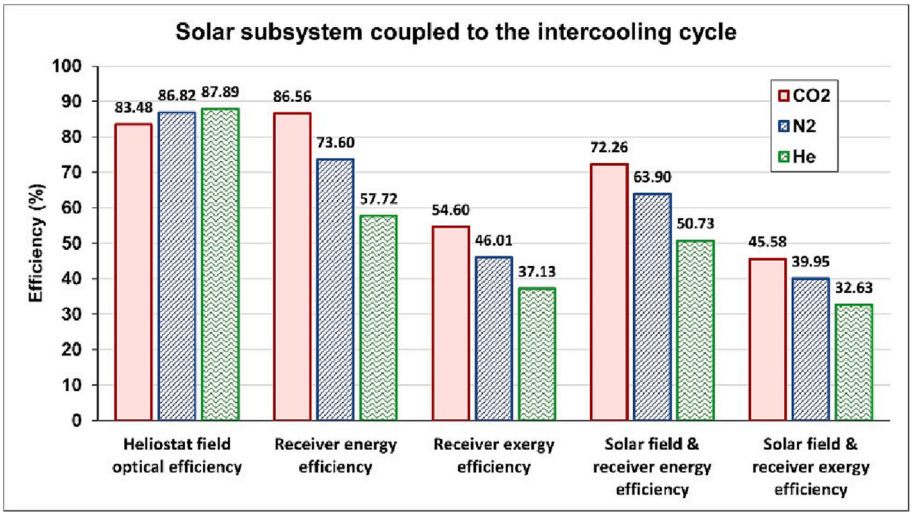

b

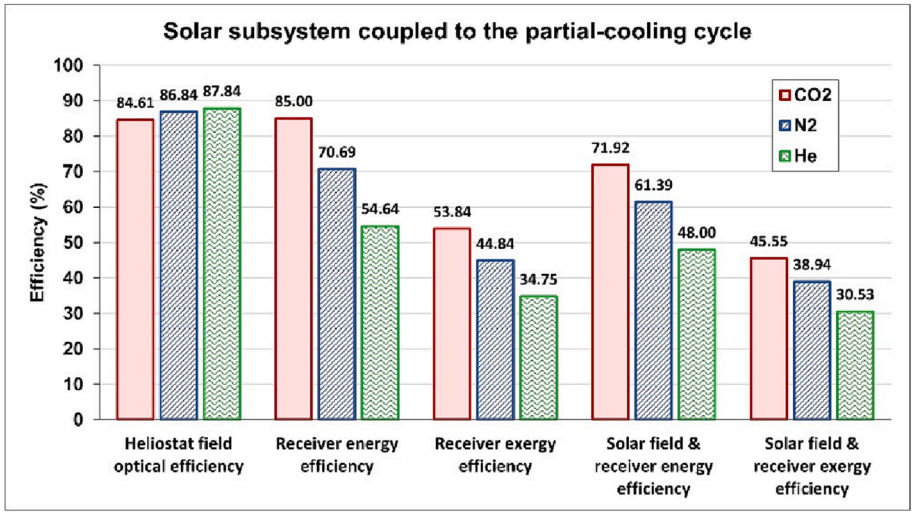

c

Fig. 11. Optical and thermal performance of the solar subsystem indirectly coupled to each sCO_2 cycle, as function of the heat transfer fluid in the receiver (CO_2, N_2 or He) (a) Recompression (b) Intercooling (c) Partial-cooling.

Table 8
Summary of the fixed capital investments for the solar subsystem of each optimised solar thermal power plant, based on a sCO_2 cycle.

	Recompresssion	Intercooling	Partial-cooling	Direct coupling
Design parameters				
Tower height (m)	108.373	107.450	103.420	108.210
Receiver absorber area (m^2)	424.839	410.140	490.195	514.377
Number of heliostats	1243	1199	1264	1346
Economic parameters				
Tower cost (Mio. $)	10.209	10.103	10.281	10.190
Receiver cost (Mio.$)	20.618	20.116	22.790	23.571
Site improvements cost (Mio. $)	2.871	2.770	2.920	3.109
Heliostat field cost (Mio. $)	26.021	25.100	26.461	28.178
Contingency cost (Mio. $)	4.238	4.124	4.435	3.938
Total direct cost (Mio. $)	63.957	62.212	66.887	68.986
Land cost (Mio. $)	2.812	2.751	2.916	2.940
Sales tax cost (Mio. $)	2.703	2.631	2.828	2.526
Total indirect cost (Mio. $)	5.516	5.383	5.744	5.466
Solar field TCC (Mio. $)	69.472	67.595	72.631	74.452

Table 9
Summary of the fixed capital investments for the power cycle of each optimised solar thermal power plant, based on a sCO_2 cycle.

	Recompresssion	Intercooling	Partial-cooling	Direct coupling
Primary heat exchanger (Mio. $)	13.516	9.531	9.141	–
Recuperators (LTR + HTR) (Mio. $)	56.4	33.9	20.7	59.125
Precooler CO_2/Air (Mio. $)	6.8	11.2	11.8	10
Turbomachinery (TM) (Mio. $)	49.2	43	43	43.055
Power cycle TCC (Mio. $)	125.916	97.631	84.641	112.180

- The comparison between cycles has been carried out in two different ways. On the one hand, the solar subsystem performance has been evaluated for all STPPs based on indirect coupling, depending on the working conditions of the fluid in the solar receiver. Afterwards, all the optimum configurations have been compared, resulting that the STPP based on the intercooling cycle is the one with the highest overall efficiency, due to the higher cycle efficiency and the thermal increment characteristics in the primary heat exchanger (large increment with relatively low inlet temperature) that improve the solar subsystem efficiency (smaller receiver dimensions and lower heat losses). On the other hand, the directly coupled recompression cycle corresponds to and should be compared to the indirectly coupled conventional recompression cycle. This comparison shows that the STPP with indirect coupling presents better efficiency, since, although the cycle net efficiency is lower, the solar subsystem efficiency is higher.

Table 10
Levelised cost of energy of each optimised solar thermal power plant, based on a sCO_2 cycle.

	Recompresssion	Intercooling	Partial cooling	Direct coupling
Weighted Average Capital Cost (WACC) (%)	8	8	8	8
Economic lifetime (n) (years)	30	30	30	30
O&M costs per kWh (OMC) ($/kWh)	0.023	0.023	0.023	0.023
Capital Recovery Factor (CRF) ($year^{-1}$)	8.883	8.883	8.883	8.883
Capacity factor (CF) (%)	25	25	25	25
Annual Electricity Production (AEP) (GW_e)	90.327	94.553	93.983	108.668
Total Capital Cost (TCC) (Mio. $)	195.388	165.226	157.272	186.632
Levelised Cost of Energy (LCOE) ($/kWh_e$)	0.2151	0.1782	0.1506	0.1756

- For the same working conditions (pressure and temperature), the type of HTF in the solar subsystem is also a weighty factor in the performance of the plant. In this way, it has been demonstrated that CO_2 is preferred over N_2 or He, as it has better heat transfer characteristics in the working conditions analysed, and therefore requires a smaller absorber surface in the receiver.
- The HTF pressure at the inlet of the solar receiver also affects the overall thermal performance of the STPP. The solar receiver size decreases as the working pressure increases. This improves the receiver energy and exergy efficiencies, as it reduces the receiver dimensions and thus the heat losses and pressure drop; but it penalises the optical efficiency, as the spillage losses increase. Both factors lead to an optimum working pressure, which depends on sCO_2 cycle, as it determines the operating temperature in the solar receiver. The higher the temperature, and thus the higher the heat losses, the higher the optimum working pressure since, a reduced solar receiver size has a more significant effect on the reduction of heat losses.
- The economic analysis also identifies several items that largely affect the investment cost. On the power block side, the cost of the turbomachinery is very similar in all configurations, and the most important factor is the number and size of the heat exchangers in the cycle, mainly the recuperators, necessary in the recompression scheme, and the primary heat exchanger, included in the indirectly coupled configuration. On the solar field side, the tower height is similar for all the configurations, so the most important factors are the solar receiver size and the number of heliostats. In this sense, an increased pressure always favours a smaller solar field size, but an excessive working pressure yields to very small receiver dimensions, higher spillage loss and lower optical efficiency, thus increasing the number of heliostats.
- Finally, the analysis conducted on the LCOE shows that while the initial investment significantly influences the final levelised cost, it is also impacted by the annual power production. In this regard, the STPP with the lowest LCOE is the configuration corresponding to the indirectly coupled partial-cooling cycle, primarily due to its lower investment cost. However, it is followed closely by the direct coupled configuration. This is because the direct coupled configuration has

significantly lower self-consumption compared to the indirectly coupled configurations. This is caused by the absence of a blower in the solar loop and the CO_2 compression being performed at a lower temperature.

5. Future works

There are many future research lines from this work, including: a more detailed analysis of each of the proposed schemes, considering the detailed engineering, pipe sizing, etc.; analysis of other schemes in the direct coupling option, including intercooling, partial-cooling or reheating, and their comparison with the corresponding indirectly coupled cycles; implementation of the thermal storage system in future schemes; design of the control system of the STPP; and finally, analysis of the transient and annual assessment based on typical year data at specific locations.

CRediT authorship contribution statement

M.J. Montes: Conceptualization, Methodology, Software, Formal analysis, Validation, Investigation, Resources, Data curation, Writing – original draft, Writing – review & editing, Visualization, Supervision, Funding acquisition, Project administration. **R. Guedez:** Conceptualization, Methodology, Investigation, Formal analysis, Investigation, Resources, Writing – original draft, Writing – review & editing. **J.I. Linares:** Conceptualization, Methodology, Software, Formal analysis, Validation, Investigation, Resources, Data curation, Writing – review & editing, Visualization, Funding acquisition, Project administration. **M.A. Reyes-Belmonte:** Conceptualization, Investigation, Resources, Writing – review & editing.

Declaration of Competing Interest

The authors declare that they have no known competing financial interests or personal relationships that could have appeared to influence the work reported in this paper.

Data availability

Data will be made available on request.

Acknowledgments

The authors thank the support by the Spanish Ministry of Economy and Competitiveness through the PID2019-110283RB-C31 and PID2019-110283RB-C33 projects.

References

[1] Irena. Renewable Power Generation Costs in 2021. Abu Dhabi: International Renewable Energy Agency; 2022.
[2] Mehos M, Turchi C, Vidal J, Wagner M, Ma Z, Ho C, et al. Concentrating Solar Power Gen3 Demonstration Roadmap 2017;No. NREL/TP–5500-67464:1338899). https://doi.org/10.2172/1338899.
[3] Reyes-Belmonte MA, Guédez R, Montes MJ. Bibliometric Analysis on Supercritical CO_2 Power Cycles for Concentrating Solar Power Applications. Entropy 2021;23:1289. https://doi.org/10.3390/e23101289.
[4] Montes MJ, Linares JI, Barbero R, Moratilla BY. Optimization of a new design of molten salt-to-CO_2 heat exchanger using exergy destruction minimization. Entropy 2020;22:883. https://doi.org/10.3390/E22080883.
[5] Montes MJ, Linares JI, Barbero R, Rovira A. Proposal of a new design of source heat exchanger for the technical feasibility of solar thermal plants coupled to supercritical power cycles. Sol Energy 2020;211:1027–41. https://doi.org/10.1016/j.solener.2020.10.042.
[6] Kelly B, Izygon M, Vant-Hull L. Advanced Thermal Energy Storage for Central Receivers with supercritical coolants. SolarPaces Conf 2010. https://doi.org/10.2172/981926.
[7] Johnson E, Bates L, Dower A, Bueno PC, Anderson R. Thermal energy storage with supercritical carbon dioxide in a packed bed: Modeling charge-discharge cycles. J Supercrit Fluids 2018;137:57–65. https://doi.org/10.1016/j.supflu.2018.03.009.
[8] Wang K, He Y-L, Zhu H-H. Integration between supercritical CO2 Brayton cycles and molten salt solar power towers: A review and a comprehensive comparison of different cycle layouts. Appl Energy 2017;195:819–36. https://doi.org/10.1016/j.apenergy.2017.03.099.
[9] Wang K, He YL. Thermodynamic analysis and optimization of a molten salt solar power tower integrated with a recompression supercritical CO_2 Brayton cycle based on integrated modeling. Energy Convers Manag 2017;135:336–50. https://doi.org/10.1016/j.enconman.2016.12.085.
[10] Turchi CS, Vidal J, Bauer M. Molten salt power towers operating at 600–650 °C: Salt selection and cost benefits. Sol Energy 2018;164:38–46. https://doi.org/10.1016/j.solener.2018.01.063.
[11] Chen R, Romero M, González-Aguilar J, Rovense F, Rao Z, Liao S. Optical and thermal integration analysis of supercritical CO2 Brayton cycles with a particle-based solar thermal plant based on annual performance. Renew Energy 2022;189:164–79. https://doi.org/10.1016/j.renene.2022.02.059.
[12] Buck R, Sment J. Techno-economic analysis of multi-tower solar particle power plants. Sol Energy 2023;254:112–22. https://doi.org/10.1016/j.solener.2023.02.045.
[13] Ho C. A review of high-temperature particle receivers for concentrating solar power. Appl Therm Eng 2016;109:958–69. https://doi.org/10.1016/j.applthermaleng.2016.04.103.
[14] Reyes-Belmonte MA, Rovense F. High-Efficiency Power Cycles for Particle-Based Concentrating Solar Power Plants: Thermodynamic Optimization and Critical Comparison. Energies 2022;15:8579. https://doi.org/10.3390/en15228579.
[15] Fernández-Torrijos M, Albrecht KJ, Ho CK. Dynamic modeling of a particle/supercritical CO_2 heat exchanger for transient analysis and control. Appl Energy 2018;226:595–606. https://doi.org/10.1016/j.apenergy.2018.06.016.
[16] Zhang HL, Benoit H, Gauthier D, Degrève J, Baeyens J, López IP, et al. Particle circulation loops in solar energy capture and storage: Gas–solid flow and heat transfer considerations. Appl Energy 2016;161:206–24. https://doi.org/10.1016/j.apenergy.2015.10.005.
[17] Ho CK. Advances in central receivers for concentrating solar applications. Sol Energy 2017. https://doi.org/10.1016/j.solener.2017.03.048.
[18] Li MJ, Li MJ, Ma Z, Yuan F. Comparisons of thermal performance and cost for three thermal energy storage systems utilized in supercritical CO_2 Brayton cycle. Energy Procedia 2019;158:4696–701. https://doi.org/10.1016/j.egypro.2019.01.734.
[19] Trevisan S, Guédez R, Laumert B. Supercritical CO_2 Brayton power cycle for CSP with packed bed TES integration and cost benchmark evaluation. In Proceedings of the American Society of Mechanical Engineers, Power Division (Publication) POWER; American Society of Mechanical Engineers (ASME), 2019; Vol. 2019-July.
[20] Heller P, Jedamski J, Amsbeck L, Uhlig R, Ebert M, Svensson M, et al. Development of a solar-hybrid microturbine system for a mini-tower. In: Proceedings of SolarPACES 2009, Berlin, Germany, September 15–18, 2009.
[21] Amsbeck L, Denk T, Ebert M, Gertig C, Heller P, Herrmann P, et al. Test of a solar-hybrid microturbine system and evaluation of storage deployment. In: Proceedings of SolarPACES 2010, Perpignan, France, September 21–24, 2010.
[22] Christian JM, Ortega JD, Ho CK, Yellowhair J. Design and modeling of light-trapping tubular receiver panels. In: Proceedings of the ASME 2016 Power and Energy Conference, PowerEnergy2016-59158, Charlotte, North Carolina, June 26–30, 2016.
[23] Hesselgreaves JE. Compact heat exchangers: selection, design, and operation. 2nd ed. Amsterdam: Elsevier/BH; 2017.
[24] Li Q, Flamant G, Yuan X, Neveu P, Luo L. Compact heat exchangers: A review and future applications for a new generation of high temperature solar receivers. Renew Sustain Energy Rev 2011;15:4855–75. https://doi.org/10.1016/j.rser.2011.07.066.
[25] Li Q, de Tourville NG, Yadroitsev I, Yuan X, Flamant G. Micro-channel pressurized-air solar receiver based on compact heat exchanger concept. Sol Energy 2013;91:186–95. https://doi.org/10.1016/j.solener.2013.02.004.
[26] L'Estrange T, Truong E, Rymal C, Rasouli E, Narayanan V, Apte S, Drost K. High flux microscale solar thermal receiver for supercritical carbon dioxide cycles. In: Proceedings of the Asme 13th International Conference on Nanochannels, Microchannels, and Minichannels; 2015.
[27] Besarati SM, Goswami DY, Stefanakos EK. Development of a Solar Receiver Based on Compact Heat Exchanger Technology for Supercritical Carbon Dioxide Power Cycles. J Sol Energy Eng 2015;137:031018. https://doi.org/10.1115/1.4029861.
[28] Sullivan SD, Kesseli J, Nash J, Farias J, Kesseli D, Caruso W. High-Efficiency Low-Cost Solar Receiver for Use Ina a Supercritical CO2 Recompression Cycle (No. DOE-BRAYTON–0005799, 1333813); 2016, doi: 10.2172/1333813.
[29] Montes MJ, Rovira A, González-Aguilar J, Romero M. Solar receiver consisting of absorber panels based on compact structures. Spanish Patent ES2911108. PCT application n. PCT/ES2022/070705. Eu. application n. 2023/10572; 2022.
[30] Montes MJ, D'Souza D, Linares JI, González-Aguilar J, Romero M. Proposal of a novel design of microchannel central solar receiver for pressurised gases and supercritical fluids. Int J Therm Sci 2023.
[31] Montes MJ, D'Souza D, Linares JI, González-Aguilar J, Rovira A, Romero M. Proposal of a Microchannel Receiver for Pressurised Fluids Based on Different Compact Geometries. Presented at the SOLARPACES 2022: International Conference on Concentrating Solar Power and Chemical Energy Systems, Albuquerque, USA; 2022.
[32] Dostal VA. Supercritical Carbon Dioxide Cycle for Next Generation Nuclear Reactors, Massachusetts Institute of Technology (MIT), Cambridge, MA; 2004.
[33] Neises T, Turchi C. Supercritical carbon dioxide power cycle design and configuration optimization to minimize levelized cost of energy of molten salt power towers operating at 650 °C. Sol Energy 2019;181:27–36. https://doi.org/10.1016/j.solener.2019.01.078.

[34] Linares JI, Montes MJ, Cantizano A, Sánchez C. A novel supercritical CO_2 recompression Brayton power cycle for power tower concentrating solar plants. Appl Energy 2020;263:114644. https://doi.org/10.1016/j.apenergy.2020.114644.
[35] MATLAB & Simulink – MathWorks; 2022. https://matlab.mathworks.com.
[36] D'Souza D, Montes MJ, Romero M, González-Aguilar J. Energy and exergy analysis of microchannel central solar receivers for pressurised fluids. Appl Therm Eng 2023;219:119638. https://doi.org/10.1016/j.applthermaleng.2022.119638.
[37] SolarPACES; 2023. https://www.solarpaces.org/.
[38] Medrano M, Puente D, Arenaza E, Herrazti B, Paule A, Brañas B, et al. Power conversion cycles study for He-cooled reactor concepts for DEMO. Fusion Eng Des 2007;82:2689–95. https://doi.org/10.1016/j.fusengdes.2007.04.041.
[39] NIST database https://webbook.nist.gov/chemistry/.
[40] Stalin Maria Jebamalai J. Receiver Design Methodology for Solar Tower Power Plants. Master Thesis. KTH School of Industrial Engineering and Management; 2016. Retrieved from http://urn.kb.se/resolve?urn=urn:nbn:se:kth:diva-192664.
[41] Ho CK, Iverson BD. Review of high-temperature central receiver designs for concentrating solar power. Renew Sustain Energy Rev 2014;29:835–46. https://doi.org/10.1016/j.rser.2013.08.099.
[42] Wagner MJ, Wendelin T. SolarPILOT: A power tower solar field layout and characterization tool. Sol Energy 2018;171:185–96. https://doi.org/10.1016/j.solener.2018.06.063.
[43] Wendelin T. SolTRACE: A New Optical Modeling Tool for Concentrating Solar Optics. Proceedings of the ISEC 2003: International Solar Energy Conference, 15-18 March 2003, Kohala Coast, Hawaii. New York: American Society of Mechanical Engineers, NREL Report No. CP-550-32866; 2003, pp. 253-260.
[44] Parrott JE. Theoretical upper limit to the conversion efficiency of solar energy. Sol Energy 1978;21(3):227–9.
[45] Bejan A, Tsatsaronis G, Moran M. Thermal Design & Optimization. Wiley; 1996.
[46] Montes MJ, Rovira A, Muñoz M, Martínez-Val JM. Performance analysis of an Integrated Solar Combined Cycle using Direct Steam Generation in parabolic trough collectors. Appl Energy 2011;88:3228–38. https://doi.org/10.1016/j.apenergy.2011.03.038.
[47] Short W, Packey DJ, Holt T. A manual for the economic evaluation of energy efficiency and renewable energy technologies. United States 1995;N. p. https://doi.org/10.2172/35391. Web.
[48] Fleming DD, Holschuh, Thomas Vernon, Conboy TM, Pasch JJ, Wright SA, Rochau GE, Fuller RL. Scaling considerations for a multi-megawatt class supercritical CO_2 brayton cycle and commercialization. (No. SAND2013-9106, 1111079); 2013, doi: 10.2172/1111079.
[49] Islam T, Huda N, Abdullah AB, Saidur R. A comprehensive review of state-of-the art concentrating solar power (CSP) technologies: current status and research trends. Renew Sustain Energy Rev 2018;91:987–1018. https://doi.org/10.1016/j.rser.2018.04.097.
[50] Gutiérrez RE, Haro P, Gómez-Barea A. Techno-economic and operational assessment of concentrated solar power plants with a dual supporting system. Appl Energy 2021;302:117600. https://doi.org/10.1016/j.apenergy.2021.117600.